ELSEVIER

Advances in Colloid and Interface Science
71–72 (1997) 125–145

ADVANCES IN COLLOID AND INTERFACE SCIENCE

Electrical functional properties of surface superstructures on semiconductors

Shuji Hasegawa* Chun-Sheng Jiang, Xiao Tong, Yuji Nakajima

Department of Physics, School of Science, University of Tokyo, 7-3-1 Hongo, Bunkyo-ku, Tokyo 113, Japan

Abstract

We have found that the electrical conductivity parallel to the surface of a bulk silicon crystal is crucially influenced by the surface superstructures formed only on the topmost atomic layers of the surface. We have demonstrated this influence by depositing metal (Au, Ag, Cu, Pb, or In) on Si(111) surfaces that had a variety of surface superstructures such as Si(111)-7 × 7 clean, $\sqrt{3} \times \sqrt{3}$, 5 × 2, and so on. The increase in surface electrical conductance compared with the clean Si(111) surface were due either to conduction through the surface space-charge layer, to the two-dimensional surface-state bands, or to the conductive metal layers grown on the surface, depending on the combination of the deposit and the substrate-surface structure. This is the first investigation directly correlating the electrical conductivity to the surface structures. This result may lead to nanometer-scale electronic devices that use the electrical conduction restricted within a few atomic layers on the surface with controlled domains of surface superstructures. © 1997 Elsevier Science B.V.

Keywords: Surface superstructures; Surface conductivity; Silicon; Electron diffraction; Photoemission spectroscopy

Introduction

Silicon surfaces have been prime targets in modern surface science, which now routinely resolves geometric and electronic structures of such surfaces at an atomic

* Corresponding author. PRESTO, Research Development Corporation of Japan (JRDC).

PII S0001-8686(97)00014-6

level. Techniques are now used not only to analyze surfaces, but also to control them atom by atom. In particular, recent STM (scanning tunneling microscopy) techniques allow us to 'manipulate' individual atoms adsorbed on the surface, thus opening up the possibility of constructing ultimate nanometer-scale structures on a surface [1]. Therefore, this is an opportune time for correlating atomic-level surface-structural modifications with the electrical properties. In this context we have studied the electrical properties of silicon surfaces of which structures are controlled at an atomic level [2]. But we have not used the STM method for structural modifications, but instead have used surface reconstruction, which is a kind of self-organization phenomena, and the resulting superstructures. A silicon (111) surface exhibits a wide variety of superstructures by foreign-atom adsorption in which the coverage ranges from sub-monolayer to several atomic layers; the resulting surface-electronic states differ greatly. For this reason, silicon surfaces provide a good playground for our investigations.

Electrical conduction near semiconductor surfaces is generally classified into three types, each of which is in principle closely related to the surface structure [3]:

(1) Conduction via a surface space-charge layer. Excess charges trapped in the surface states cause band-bending below it, resulting in changes in carrier concentrations in the space-charge layer, whose width reaches several microns in a lightly-doped semiconductor substrate. The surface electronic states of each superstructure thus can decisively govern the electrical conductivity through the layer.
(2) Conduction via surface-state bands. Two-dimensional bands are formed due to the surface superstructure. The electrons in these bands should be mobile along the surface, just like the electrons in the three-dimensional bulk bands, so that they contribute to electrical conduction. Conductivity of this type is directly dependent on the nature of the surface-state band (metallic or semiconducting) and the effective mass of the carriers therein.
(3) Conduction via a grown atomic layer. If, for example, metal atomic layers grow on a semiconductor surface at low temperatures, the grown layers dominate the conduction above a percolation-threshold coverage [4]. Diffusivity of carrier scattering at the surface and the interface depends on the morphology of the growing surface, leading to changes in carrier mobility. Therefore, the conductivity is sensitive to the growth modes and kinetics, both of which are dependent on the surface structure. Although conduction through thin films has been extensively studied for the past 50 years [5], our interest lies in the thickness range from sub-monolayer to a few atomic layers where the structures of the substrate surface as well as the growth modes decisively affect the conductivity [6].

To extract the surface contribution from the measured conductivity, which also includes the bulk contribution, the conductivity changes should be measured in situ in a controlled manner in UHV (ultra-high vacuum) during modifications of surfaces. To do this, we have used the following three methods:

(1) Adsorption of (foreign) atoms. Adsorbed atoms can have excess charges, bringing about band-bending below the surface, or can induce a new surface reconstruction that generates completely different surface electronic states.
(2) Application of external electric field (surface-field effect). The field applied normal to the surface can penetrate the semiconductor, giving rise to band-bending. But the field can be screened to be prevented from penetration by metallic surface states, if any.
(3) Irradiation with light. Excitation and re-combination of carriers near the surface can proceed through the surface states, especially for irradiation of light of less than the band-gap energy.

Only the first method will be discussed in this paper because of the limited space; the results of the latter two methods will be published elsewhere.

We first introduce the surface superstructures dealt with in this paper, Si(111)-7 $\times$ 7 clean, -$\sqrt{3}$ $\times$ $\sqrt{3}$-Ag, and -5 $\times$ 2-Au surfaces. Next, we discuss the differences in surface electrical conductance among these superstructures. Finally, we show the changes in atomic and electronic structures during Ag or Au depositions onto the respective surfaces and the resulting changes in electrical conductance.

2. Three superstructures on Si(111) surfaces

More than 300 kinds of surface superstructures have been found on silicon surfaces with foreign-atom adsorptions in which the coverage ranges from sub-monolayer to several atomic layers [7]. Most of these superstructures have not yet had their structure and nature clarified in detail. We used three of these structures for our conductivity investigations (Fig. 1): Si(111)-7 $\times$ 7, Si(111)-$\sqrt{3}$ $\times$ $\sqrt{3}$-Ag, and Si(111)-5 $\times$ 2-Au surfaces, the former two we have now fully detailed.

The first surface we used was a clean Si(111)-7 $\times$ 7 surface. Fig. 1a shows its RHEED (reflection-high-energy electron diffraction) pattern, which was prepared by usual procedures, namely, several flashings up to 1500 K followed by gradual cooling down to room temperature (RT) in UHV. The atomic arrangement of this surface is now clarified as the well-known DAS (dimer-adatom-stacking fault) structure (Fig. 1b) [8]. On its topmost layer, the DAS structure has 12 Si adatoms, which have dangling bonds that bring about a half-filled surface-electronic state as indicated by the S_1 peak in Fig. 1c; this state is indicative of a metallic character [9]. The S_1 state pins the Fermi level E_F at the surface due to its large density of states. The Fermi level is then always located around the middle of the band gap, meaning that the surface space-charge layer always exhibits a depletion layer, irrespective of the doping type of the bulk Si [10].

The second surface structure we used was the Si(111)-$\sqrt{3}$ $\times$ $\sqrt{3}$-Ag (Fig. 1d), which was formed by depositing 1 ML (monolayer) of Ag onto the clean 7 $\times$ 7 surface at a substrate temperature above 520 K. The atomic arrangement of this surface is a honeycomb-chained trimer (HCT) structure where the adsorbed Ag atoms make covalent bonds with the substrate Si atoms, leaving no dangling bonds

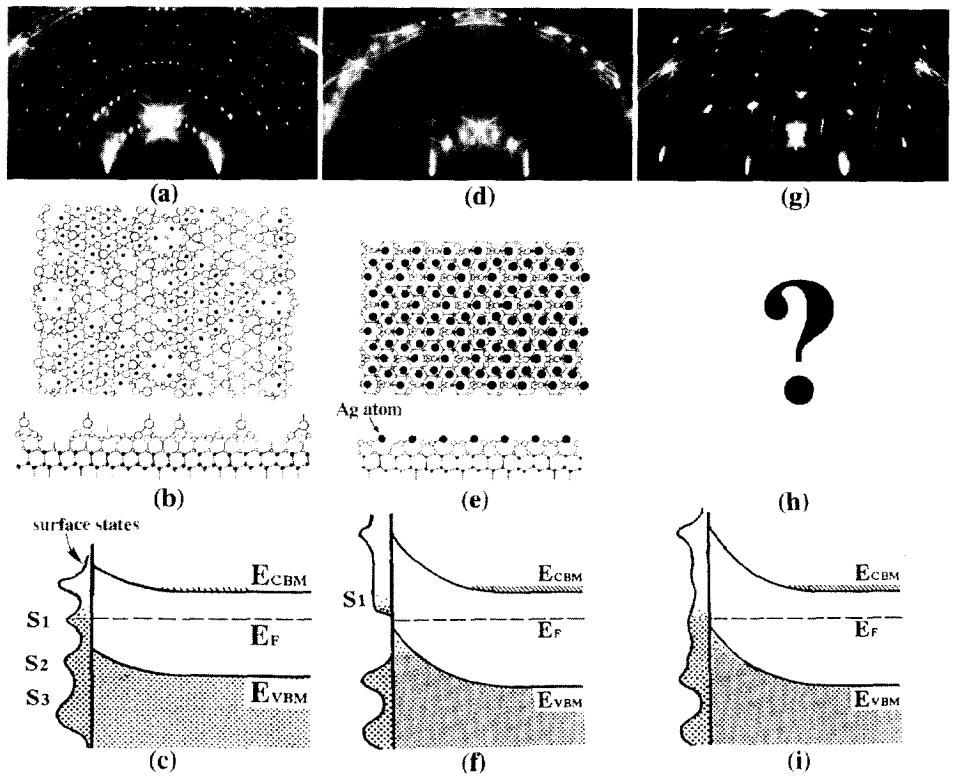

Fig. 1. Three types of surface superstructures on a Si(111) surface: (a) (b) (c) a 7 × 7 clean surface, (d) (e) (f) a $\sqrt{3} \times \sqrt{3}$-Ag surface, and (g) (h) (i) a 5 × 2-Au surface. (a) (d) (g) RHEED patterns in [112] incidence, (b) (e) atomic arrangements (plane and sectional views), and (c) (f) (i) schematic energy-band diagrams near the surfaces of an *n*-type Si crystal. E_F: Fermi level, E_{CBM}: conduction-band minimum, E_{VBM}: valence-band maximum. $S_1 \sim S_2$ in (c) and (f) indicate the surface electronic states already identified.

(Fig. 1e) [11]. It results in an extreme reduction in surface energy [12]. A distinct energy gap in the surface band structure is opened, indicating a semiconducting character (Fig. 1f) [13,14], in contrast to the metallic nature of the 7 × 7 surface. This suface has a characteristic surface-state band, named again S_1-state band. The minimum of this band is just above the E_F at the $\bar{\Gamma}$ point in the surface Brillouin zone [15], which is reproduced by the first-principles calculations [16]. So the number of the electrons thermally excited into this surface-state band are not enough to give rise to the photoemission intensity. But, as seen in the next section, these electrons can contribute to the electrical conduction parallel to the surface, because the S_1-state band is highly dispersive. Photoemission spectroscopy shows that the E_F at the surface is always located near the valence-band maximum so that the surface space-charge layer is a hole-accumulation layer (upward band-

bending), irrespective of the bulk doping type [17]. This upward surface band bending is raised by the excess electrons trapped in the S_1-state band.

The third surface we used was Si(111)-5 × 2-Au (Fig. 1g) prepared by depositing a 0.4 ML of Au onto the clean 7 × 7 surface maintained at 950 K. A generally accepted structural model for this surface is not yet obtained, though the latest paper proposes a plausible model [18]. The electronic structure of this surface is somewhat different from that of the $\sqrt{3} \times \sqrt{3}$-Ag surface. The angle-resolved ultra-violet photoelectron spectroscopy (ARUPS) shows a peculiar feature; metallic edges in a restricted range of the emission angle are seen. Collins et al. suggest a quasi-one-dimensional metallic character of this surface [19]. According to the high-resolution measurements of soft X-ray photoemission spectroscopy (PES), again, the E_F position on the 5 × 2-Au surface should lie at 0.10 eV above the VBM [20]. This means the bands bend upwards enough to create a hole-accumulation condition in the surface space-charge layer (Fig. 1i), as in the case of the $\sqrt{3} \times \sqrt{3}$-Ag surface.

These atomic and electronic structures characteristic to each surface actually give rise to decisive differences in macroscopic electrical conduction.

3. Electrical conductance of the respective surfaces

Measuring the surface conductance of surfaces with superstructures is not straightforward, because the concentration and distribution of dopants in the bulk may change due to the high-temperature heating that is necessary in the cleaning and preparation of the superstructures [21,22]. This inevitably results in changes in both surface and bulk conductivities. To extract the surface contribution from the measured conductivity with a bulk crystal, we made two types of superstructures simultaneously on a single Si(111) wafer (one superstructure on each half of the wafer), and measured the conductivity of the respective surface areas at one time. The bulk beneath the superstructures should have the same heating histories and temperature, meaning the same bulk conductivity. So the difference in the measured conductivity can be attributed only to the difference in the surface conductance [23].

Figure 2 shows a schematic of the sample holder for the conductivity measurements and RHEED observations. During the Ag or Au depositions in the preparation of the respective structures, one-half of the wafer was covered by a mask to prevent from metal adsorption, while the whole wafer was heated to a uniform temperature. The structure of the other half was changed into either the $\sqrt{3} \times \sqrt{3}$-Ag or 5 × 2-Au structure, while the masked area remained the clean 7 × 7 structure. The differential resistance of the respective areas were simultaneously measured by monitoring the voltage drops between two pairs of Ta wire contacts set on each respective surface area, by changing the current flowing through the Ta clamps at both ends of the wafer. By averaging several measurements for a *p*-type Si(111) wafer with resistivity of 20 Ω cm and size of 40 × 5 × 0.4 mm^3, we

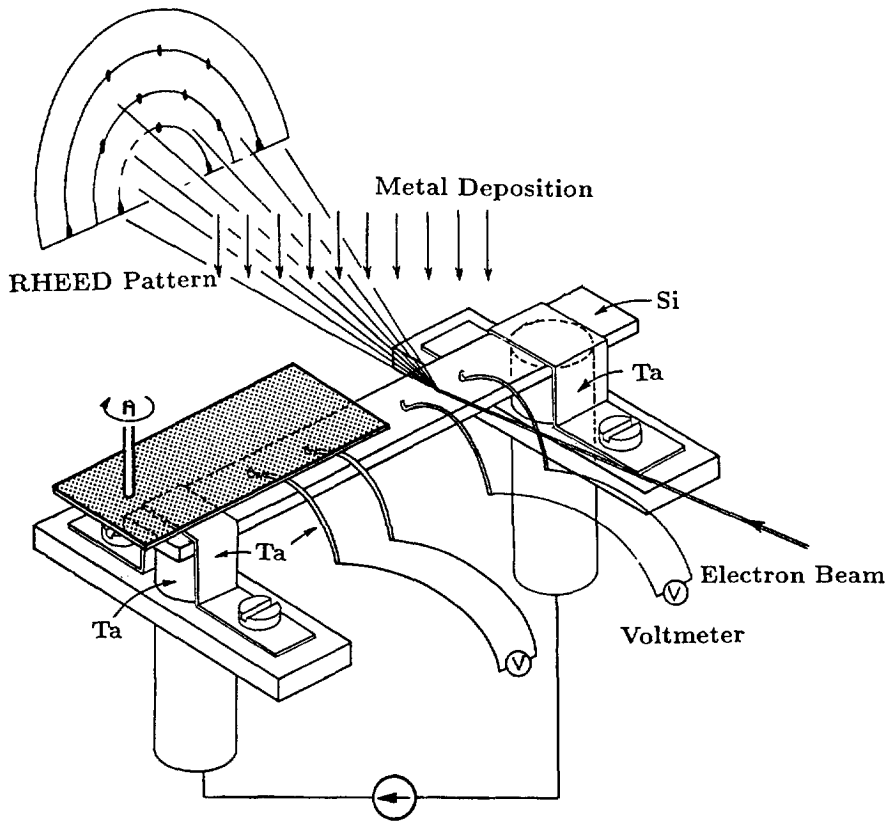

Fig. 2. RHEED sample holder for the electrical conductivity measurements using a four-probe method. After the surface superstructures were confirmed by using RHEED, the electron beam was turned off during the subsequent conductivity measurements.

determined the conductivity for the 7×7, $\sqrt{3} \times \sqrt{3}$-Ag, and 5×2-Au surfaces to be 5.06, 5.35, and $5.18 \times 10^{-2}\Omega^{-1}\text{cm}^{-1}$, respectively. Because their bulk conductivities are the same, the surface conductance of the $\sqrt{3} \times \sqrt{3}$-Ag and 5×2-Au surfaces, $\sigma_{\sqrt{3}}$ and σ_5, are larger than that of the 7×7, σ_7, by $(11.5 \pm 0.5) \times 10^{-5}$ A/V and $(5 \pm 1) \times 10^{-5}$A/V, respectively [23].

We now discuss the reasons why the $\sqrt{3} \times \sqrt{3}$-Ag and 5×2-Au surfaces have higher conductances than the 7×7 clean surface. We first estimate the contribution of the surface space-charge-layer. Since the measured conductivity of the Si wafer with the 7×7 structure was 5.06×10^{-2} Ω^{-1} cm $^{-1}$ which was consistent with the initial resistivity of 20 Ω cm, the doping profile near the surface region of our p-type samples was not considered to be significantly changed by the high-temperature treatments. The E_F position in the bulk is then estimated to be located at 0.29 eV above the valence-band maximum (VBM). If the E_F position at the surface is given, the electrical field (band bending) and carrier density in the surface

space-charge layer can be calculated by solving the Poisson equation by assuming a uniform distribution of impurity throughout the layer. The conductivity through the layer was then calculated [24], using the bulk parameters of the hole mobility, 495 cm^2/V s, and the electron mobility, 1330 cm^2/V s. The result is shown in Fig. 3 as a function of the surface E_F position.

It is known that the surface E_F of the 7×7 structure lies at 0.63 eV above the VBM, irrespective of the bulk impurity concentration [10]. This means a very low conductivity through the surface space-charge layer from Fig. 3, i.e., a depletion layer below the 7×7 structure. As mentioned in Section 2, the E_F position on the 5×2-Au surface should lie at 0.10 eV above the VBM [20]. By plotting this E_F position on Fig. 3, the conductivity should increase by about 4×10^{-5} A/V compared with the 7×7 surface. This value seems consistent with our measured excess conductivity, $(5 \pm 1) \times 10^{-5}$ A/V. Therefore it can be said that the excess surface electrical conductance for the 5×2-Au structure is mainly attributed to the surface space-charge layer.

For the $\sqrt{3} \times \sqrt{3}$-Ag surface, again, the surface E_F lies at 0.10 eV above the VBM [17]. Then, the excess conductance estimated from Fig. 3 is 4×10^{-5} A/V,

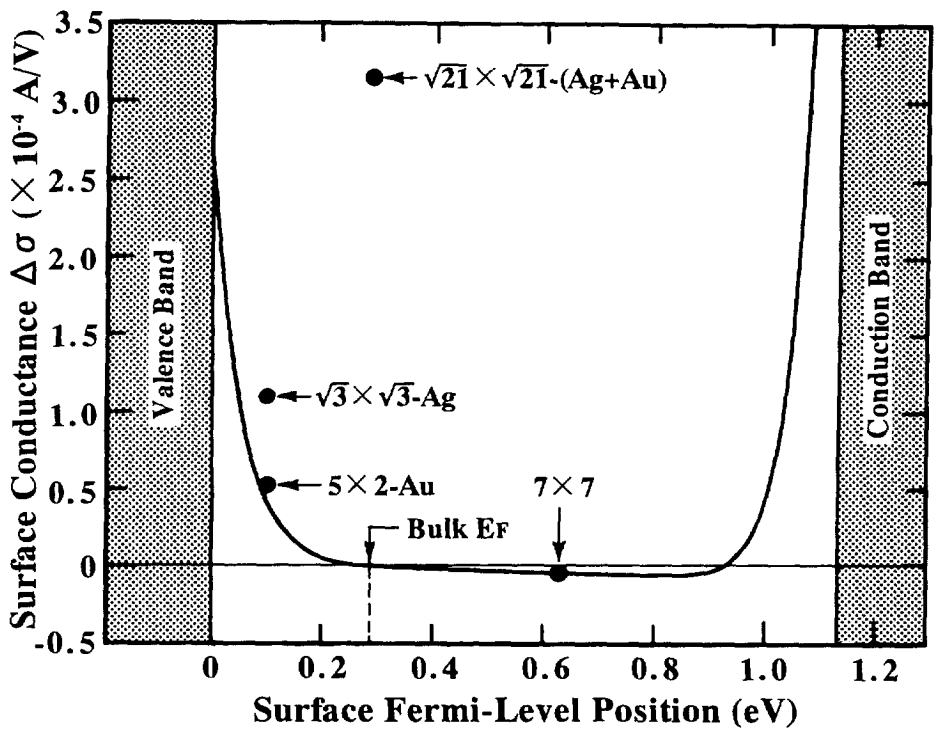

Fig. 3. Calculated surface conductivity through the surface space-charge layer as a function of the surface Fermi-level position using the valence-band maximum as a reference. The mobility of each carrier was assumed to be equal to that in the bulk crystal. The inserts are schematics of the bands.

which is too small to explain our measured value, 1.1×10^{-4} A/V. Though this discrepancy may partly come from the unrefined assumptions (a uniform distribution of the dopants and the bulk mobility values) for the estimation of the curve in Fig. 3, we need other reasons to explain the larger discrepancy compared with the 5×2-Au case.

We next discuss the contribution of other two types of conductions, i.e., through the grown metal layer and through the surface-state bands. The saturation coverage of Au for the 5×2 phase is 0.4 ML [18], which is too small to be regarded as a metal Au layer grown on the surface. In fact, as mentioned in Section 2, a quasi-one-dimensional metallic character of this surface is observed [19]. So there is a possibility that a part of the excess surface electrical conductivity of the 5×2-Au surface is attributed to this quasi-one-dimensional metallic surface state; the conductivity can be enhanced along the stripes with five-fold-units separation observed in images of scanning tunneling microscopy [25]. But, as mentioned above, this contribution could not be confirmed by our measurements and analysis, probably because our sample surfaces were composed of mixture of the 5×2-structure domains with three different orientations.

As described in Section 2, though the $\sqrt{3} \times \sqrt{3}$-Ag surface is inherently semiconductor-like, it has a strongly dispersive surface-state (S_1 state) band crossing the E_F, of which minimum is close to the E_F. So the electrons thermally excited into this surface-state band can contribute to the electrical conduction, because the S_1-state band is highly dispersive. So for the $\sqrt{3} \times \sqrt{3}$-Ag surface, the measured excess conductance above the calculated curve in Fig. 3 is considered to be attributed to this surface-state band. The surface charging, which is the origin of the upward band bending below this surface, is naturally understood by considering the excess electrons in this S_1-surface-state band [15].

Finally we should comment on the 7×7 clean surface. This surface is well known to be metallic due to the dangling bonds of the topmost surface atoms [9]. But its surface conductivity was lower than that of the $\sqrt{3} \times \sqrt{3}$-Ag surface, of which electronic structure is inherently semiconductor-like. This means that the conduction via the metallic surface-state band of the 7×7 structure is not high enough to surpass the excess conductivities through the surface space-charge layer and the surface-state S_1 band of the $\sqrt{3} \times \sqrt{3}$-Ag surface. This may be because the dispersion of the metallic band of the 7×7 surface is so small (less than 0.1 eV) that the electrons with a large effective mass in the band are almost localized on the dangling bonds of the surface atoms.

In conclusion, the surface conductivities for the Si(111)-$\sqrt{3} \times \sqrt{3}$-Ag and 5×2-Au structures were measured to be larger than that of the 7×7 clean surface. This result was qualitatively confirmed also with *n*-type Si wafers. We have thus found for the first time that the reconstructions only in one or two atomic layers on the surface actually raise the inherent changes in the macroscopic electrical conduction. The excess conductivities were explained mainly through the surface space-charge layer. But the surface-state-band conduction is considered to partly contribute, especially on the $\sqrt{3} \times \sqrt{3}$-Ag surface. In spite of a report insisting the

detection of the surface-states conduction on the 7 × 7 surface [26], we could not confirm its contribution.

4. Changes in electrical conductance during additional metal depositions onto the surfaces

Using a similar sample holder as in Fig. 2, but without a mask, we continuously measured the resistance changes of the Si wafer during metal depositions onto its surface with various surface superstructures at room temperature (RT). The structural changes in the course of deposition were monitored by RHEED observations in separate runs of depositions (the RHEED electron beam seriously disturbed the electrical measurements). We did the experiments using both n-type (resistivity = 50 ~ 100 Ω cm) and *p*-type (8 ~ 20 Ω cm) Si wafers that were 23 × 5 × 0.4 mm^3 in size. When the resistance changes are converted into the conductance changes, both types of Si wafers exhibit similar results. Since, then, the essential physics is the same for both types, we show the data at RT only for the *n*-type sample in the following sections.

4.1. For the Si(111)-7 × 7 clean surface

Figures 4a and 4b show the changes in resistance during the depositions of Au (rate = 0.21 ML/min) and Ag (0.45 ML/min), respectively, onto the clean 7 × 7 surface at RT. The changes in RHEED patterns are also indicated.

For the Au deposition, the resistance did not show significant changes at the initial deposition stage, except for a slight increase at the beginning. Above 0.8 ML coverage, the resistance began to decrease steeply, but the rate of decrease temporarily slowed down around 1.5 ML coverage. After that, the 7 × 7 spots faded away, leaving the fundamental 1 × 1 spots with increasing background intensity in RHEED. According to UHV-SEM (secondary electron microscopy) observations [27], small islands of a few nanometers in diameter appear, and then begin to coalesce with increasing Au coverage. Although it is not clear whether the islands are composed of pure Au or Au-silicide, it is natural to expect that the islands are so conductive that the electrical conduction can be set above a threshold coverage for percolation paths corresponding to the coalescence among the islands. In fact, according to the measurements of the Si-2p core-level shifts using XPS during this deposition (Fig. 4c), the E_F does not shift significantly, thus remaining in the depleted condition at the surface space-charge layer [23,28]. Therefore, the resistance drop in Fig. 4a is explained by conduction through conductive islands grown on the surface.

For the Ag deposition (Fig. 4b), the resistance changed in a way similar to that for the Au deposition; no significant change occurred until the 7 × 7 pattern disappeared around 3 ML coverage, beyond which the resistance began to decrease steeply. According to RHEED and SEM observations, the deposited Ag grows in quasi-layer-by-layer fashion up to a few monolayers, consisting of twining flat Ag

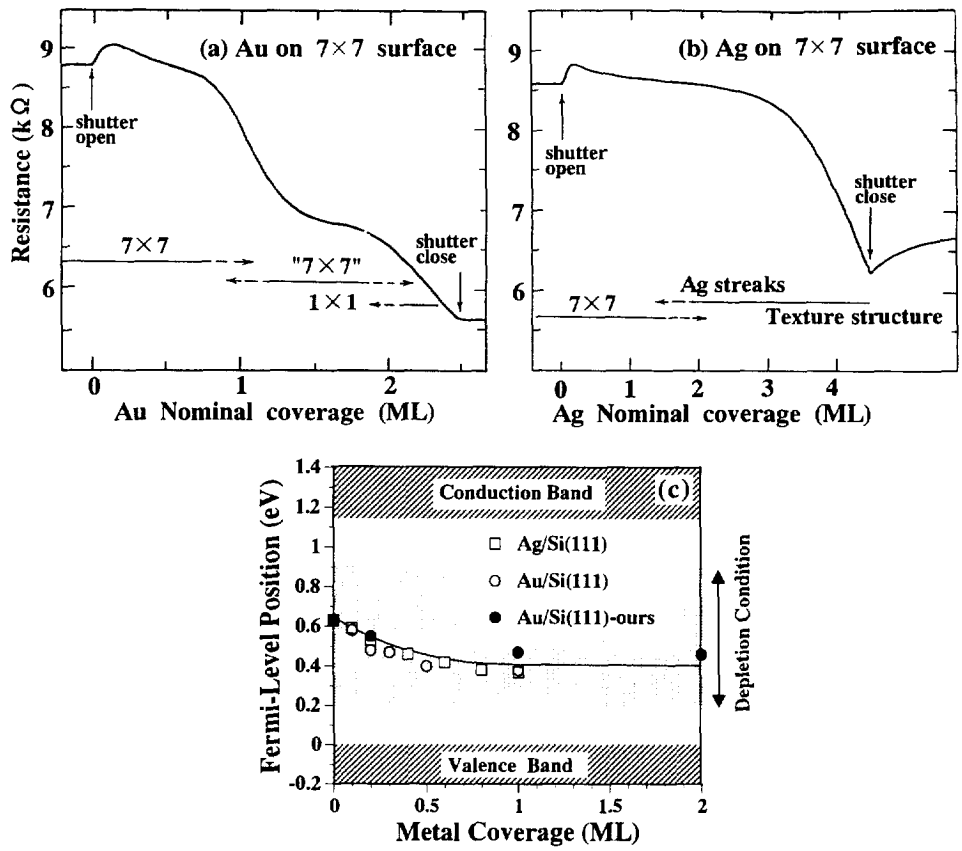

Fig. 4. Resistance changes and corresponding RHEED patterns for an Si wafer during room-temperature depositions of (a) Au and (b) Ag onto an Si(111)-7 × 7 clean surface. (c) The shifts in the surface E_F position during the metal depositions, measured by XPS. Open circles and squares are taken from the literatures [28,29], while solid circles show our measurements.

crystals in a texture structure [2]. Because a downward shift in the E_F at the surface due to this deposition was again not significant, less than 0.3 eV as shown in Fig. 4c [29], the surface space-charge layer remained depleted. So the resistance drop is explained in a way similar to that for the Au deposition; in the early stage of deposition, the Ag islands nucleated and grew without electrical connection among the islands, beyond about 3 ML coverage, however, the percolation paths were created by coalescing, leading to a steep decrease in resistance. The critical coverage for electrical connections for the Ag case was larger (about 3 ML) than that for the Au case (about 0.8 ML). This is because smaller conductive (silicide) islands were formed with the Au deposition, whereas Ag atoms tended to aggregate, thus forming larger, but fewer, islands.

In summary, the conductive metal islands grown on the surface had a dominant role in the resistance changes during deposition. The surface space-charge layer and the metallic surface-state band of the initial 7 × 7 substrate seemed to scarcely contribute to the resistance changes.

4.2. For the Si(111)-5 × 2-Au surface

Figures 5a and 5b show that the resistance changes for the 5 × 2-Au substrate surface during the Au and Ag depositions, respectively, are quite different from those for the Si(111)-7 × 7 clean surface. As soon as the deposition started, the resistance steeply increased by about 20% with only 0.2 ML coverage of additional metals. This coverage range corresponds to a minor change in the RHEED pattern; the half-order streaks in the 5 × 2 pattern (Fig. 1e) disappeared, converting into a 5 × 1 structure. Passing through the maximum, the resistance began to drop, and the 5 × 1 structure disappeared with further deposition.

Figure 6a shows the resistance change during cycles of Au deposition onto the 5 × 2-Au surface and the interruption of deposition. The resistance changes are similar to those shown in Fig. 5a during deposition periods. During the interruption periods, the resistance remained almost constant. We measured XPS spectra from Si-2p core level at each coverage by interrupting the deposition. With an additional Au coverage of 0.2 ML, corresponding to the resistance maximum in Fig. 5a, the

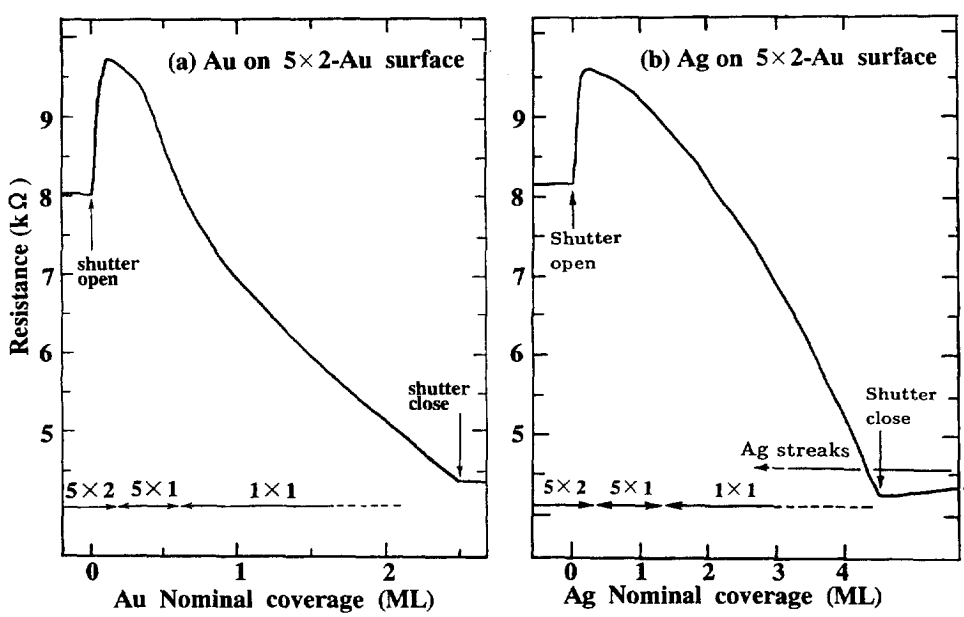

Fig. 5. Resistance changes for an Si wafer and corresponding RHEED patterns during room-temperature depositions of (a) Au and (b) Ag onto an Si(111)-5 × 2-Au surface.

core level shifted to a larger binding energy by 0.15 eV from that at the initial 5 × 2-Au surface, and returned almost to the initial position at the 1 ML coverage. As shown in Fig. 6b, this means that the E_F position at the surface shifted upwards by 0.15 eV from its initial position, and then returned to its initial position. By tracing these shifts in the surface-E_F position in Fig. 3, the change in surface conductance can be qualitatively understood in terms of changes in the surface space-charge-layer. The hole-accumulation situation at the initial 5 × 2-Au surface was converted into a depletion-layer condition by 0.2 ML-Au adsorption, resulting in a resistance increase. This means that additional Au atoms create donor-like surface electronic states to diminish the holes, in other words, to flatten the band. This same mechanism occurs in the resistance changes for the Ag adsorption (Fig. 5b).

In summary, in the early stage of both the Au and Ag depositions onto the Si(111)-5 × 2-Au surface at RT, the resistance changes can be explained by the surface space-charge layers; the initial hole-accumulation condition converts into the depletion condition by adsorption of only 0.2 ML of additional atoms, and then returns to a hole-accumulation condition by further deposition. The role of the minor structural change from the 5 × 2 into a 5 × 1 structure is not yet clear.

4.3. For the Si(111)-$\sqrt{3} \times \sqrt{3}$-Ag surface

Figure 7a shows that for Au deposition onto the $\sqrt{3} \times \sqrt{3}$-Ag surface at RT, the resistance steeply decreased dramatically by about 50% with only 0.15 ML coverage, and then recovered to about −20% around 0.5 ML coverage, beyond which the resistance monotonically decreased. A $\sqrt{21} \times \sqrt{21}$ RHEED pattern began to appear and coexist with the initial $\sqrt{3} \times \sqrt{3}$ structure from about 0.04 ML coverage, and gained its maximum intensity aound 0.15 ML, and then disappeared around 0.3 ML, changing into another $\sqrt{3} \times \sqrt{3}$ phase. The measured resistance

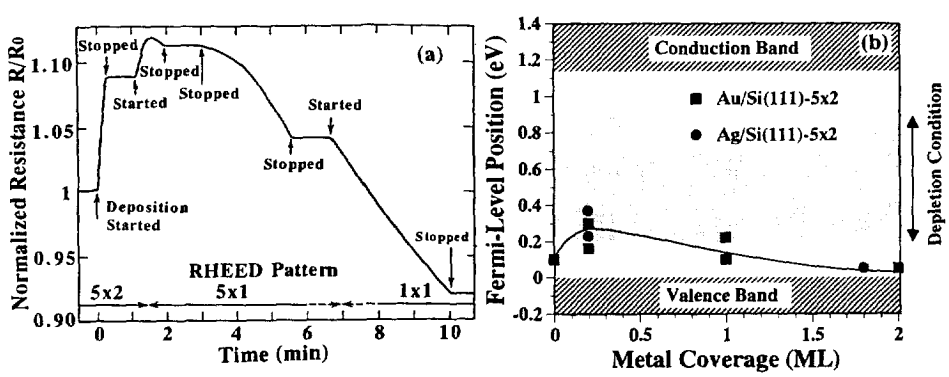

Fig. 6. (a) Resistance changes for an Si wafer with the 5 × 2-Au surface during a cycle of deposition and interruption of additional Au at RT. (b) The shifts in the surface E_F position during the metal depositions, measured by XPS.

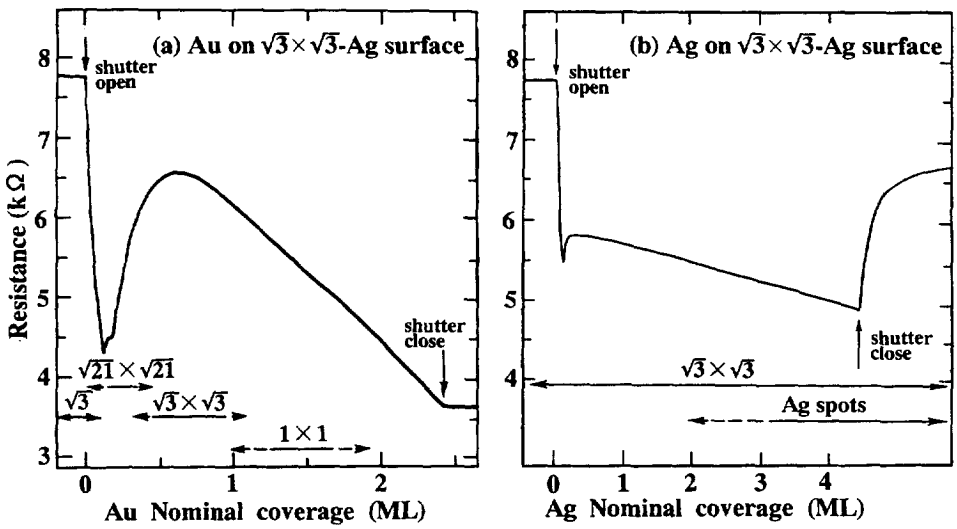

Fig. 7. Resistance changes and corresponding RHEED patterns for an Si wafer during the room-temperature depositions of (a) Au and (b) Ag onto an Si(111)-$\sqrt{3} \times \sqrt{3}$-Ag surface.

drop precisely corresponds to the emergence of this $\sqrt{21} \times \sqrt{21}$ superstructure. The maximum conductance of the $\sqrt{21} \times \sqrt{21}$-phase $\sigma_{\sqrt{21}}$ aound 0.15 ML-Au coverage is calculated from the resistance change to be larger than that of the initial $\sqrt{3} \times \sqrt{3}$-Ag surface $\sigma_{\sqrt{3}}$ by 2.0×10^{-4} A/V. This means that the surface conductance $\sigma_{\sqrt{21}}$ is larger than that of the 7×7 clean surface σ_7 by 3.2×10^{-4} A/V, because $\sigma_{\sqrt{3}}$ is larger than σ_7 by 1.2×10^{-4} A/V as measured in Section 3. This result is plotted in Fig. 3 with the E_F position in the $\sqrt{21}$-phase as mentioned below.

The intensity ratios among the fractional-order spots in the RHEED pattern of the $\sqrt{3} \times \sqrt{3}$-(Ag + Au) structure appearing around 0.5 ML-Au coverage are different from those of the initial $\sqrt{3} \times \sqrt{3}$-Ag structure; the (1/3, 1/3) spots were stronger than the (2/3, 2/3) spots, whereas the initial $\sqrt{3} \times \sqrt{3}$-Ag pattern had the opposite tendency. This means that the initial and later-appearing $\sqrt{3} \times \sqrt{3}$ structures had different atomic arrangements, despite having the same periodicity.

Again, as in the previous section, we interrupted the deposition and measured the Si 2p core-level shift by XPS during the interruption periods as a function of Au coverage. By adopting the E_F position at the initial $\sqrt{3}$-phase to be 0.1 eV above the valence-band maximum (VBM) [17], the shifts of the surface E_F position are plotted in Fig. 8a as a function of Au coverage. The E_F shifted to the bulk E_F position (0.29 eV above the VBM) with less than 0.1 ML Au adsorption, leading to a flat-band condition, which corresponded to the emergence of the $\sqrt{21}$-phase. The E_F kept almost constant with further Au deposition. By tracing this shift of the surface E_F position on the curve in Fig. 3, from 0.1 eV to 0.3 eV above the VBM,

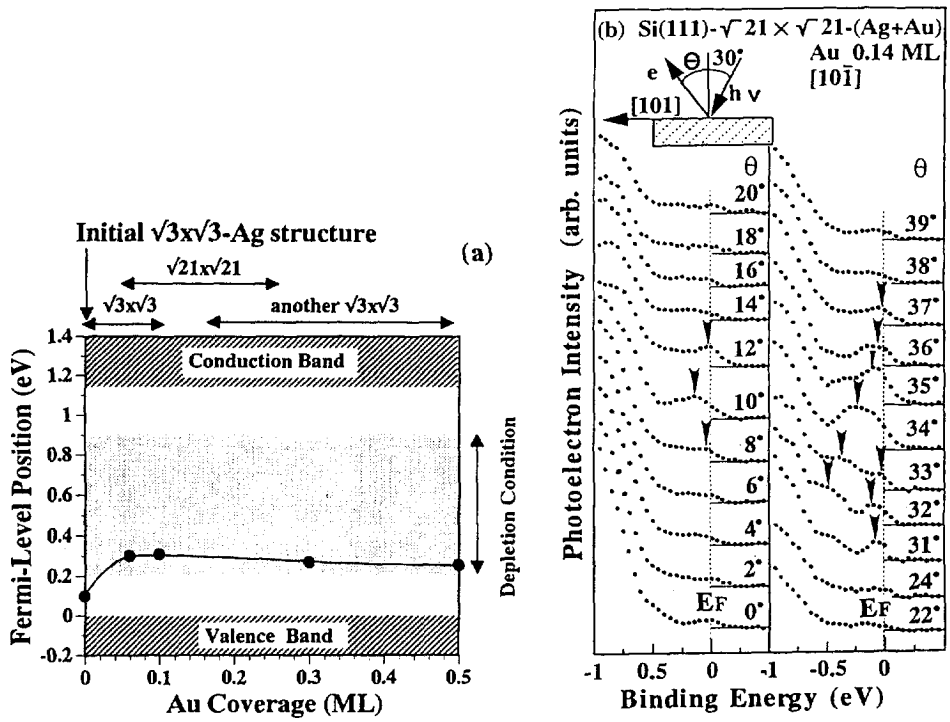

Fig. 8. (a) The shifts in the surface E_F position during the Au depositions onto the Si(111)-$\sqrt{3} \times \sqrt{3}$-Ag surface, measured by XPS. (b) Angle-resolved ultraviolet photoelectron spectra measured from the Si(111)-$\sqrt{21} \times$ superstructure induced by adsorption of additional Au of 0.14 ML onto the $\sqrt{3} \times \sqrt{3}$-Ag surface at RT. The binding energy was measured with respect to the Fermi level. Photoelectrons were detected at off-normal angles θ along the [10$\bar{1}$] direction. An unpolarized He I (21.22 eV) light was used for the excitation.

it is found that the surface space-charge layer is converted from a hole accumulated condition at the initial $\sqrt{3} \times \sqrt{3}$-Ag surface into a flat-band condition where the excess holes are depleted in accord with the structural transformation into the $\sqrt{21} \times \sqrt{21}$ phase. Then, the electrical conduction through the surface space-charge layer should be suppressed. But, on the contrary, the measured surface conductance was greatly enhanced.

ARUPS spectra near the E_F were next measured over the surface Brillouin zone for the three different surfaces, the initial $\sqrt{3} \times \sqrt{3}$-Ag surface, the $\sqrt{21} \times \sqrt{21}$ structure at 0.14 ML Au coverage, and another $\sqrt{3} \times \sqrt{3}$ phase at 0.5 ML Au coverage. For the initial $\sqrt{3}$-surface, no metallic edge at the E_F was detected at any emission angles as in the literature [13], meaning a semiconductor-like electronic structure. On the other hand, Fig. 8b shows the spectra taken from the $\sqrt{21}$-surface. Metallic edges immersing the E_F were clearly observed. Especially the peaks indicated by arrows seem to be dispersive across the E_F. This clearly shows that the

surface electronic state converted into metallic from the initial semiconductor-like with the structural transformation into the $\sqrt{21}$-phase. This metallic band seems wider than the metallic state of the 7×7 surface, indicative of smaller effective mass, which leads to an expectation of higher electrical conductivity. This may be because the $\sqrt{21} \times \sqrt{21}$ surface is much smoother than the DAS surface, an atomically rough surface.

Now, the origin of the extremely high surface conductance of the $\sqrt{21} \times \sqrt{21}$ phase can be clarified. The electrical conduction through the surface space-charge layer was excluded because of the opposite band bending as measured by XPS in Fig. 8a as mentioned before. Au of 0.14 ML coverage is too small to make percolation paths on the two-dimensional triangular lattice [4]. So we have to conclude the surface-state-band conduction that enhances the electrical conductance of the $\sqrt{21} \times \sqrt{21}$ phase.

With further Au deposition, the $\sqrt{21} \times \sqrt{21}$ structure changed into a $\sqrt{3} \times \sqrt{3}$-(Ag + Au) structure which then corresponded to a change in the electronic structure from metallic to semiconductor-like. During this change the band bending does not show any significant change as in Fig. 8a. Therefore, the increase of resistance in the Au coverages from 0.15 ML to 0.5 ML can be attributed to the effect of the suppression of the metallic surface state of the $\sqrt{21}$-phase. Over one monolayer of Au deposition, the deposited Au will exchange their atomic positions between the underlying Ag atomic layer to destroy the $\sqrt{21} \times \sqrt{21}$ periodicity [30].

For this $\sqrt{21} \times \sqrt{21}$-(Ag + Au) superstructure, Nogami et al. [31] and Ichimiya et al. [32] proposed structural models. Although the two models are for different Au coverage on top of the initial $\sqrt{3} \times \sqrt{3}$-Ag surface, 0.24 and 0.14 ML, respectively, they both have a common feature, that the initial $\sqrt{3} \times \sqrt{3}$ framework remains, thus making the $\sqrt{21} \times \sqrt{21}$ periodicity only with additional Au atoms. So the metallic surface state of this phase is considered to come from the delocalization of electrons of periodically arranged Au atoms.

Figure 7b shows that the Ag deposition, instead of Au, onto the $\sqrt{3} \times \sqrt{3}$-Ag surface at RT had a somewhat different change in resistance. After an abrupt drop in the resistance at the beginning of deposition (less than 0.1 ML coverage) and after a small overshoot, the resistance decreased at a moderate rate with further deposition. When the deposition was stopped, the resistance increased steeply. During this process, a ring pattern with some preferential-orientation spots from three-dimensional Ag micro-crystals gradually emerged in the RHEED pattern, while the initial $\sqrt{3} \times \sqrt{3}$ spots remained strong even when the Ag deposition exceeded 10 ML. This is due to the high surface diffusivity of Ag adatoms on top of the $\sqrt{3} \times \sqrt{3}$ surface, enough to nucleate into three-dimensional micro-crystals with which the surface was scarcely covered. These micro-crystals were directly observed by using UHV-SEM. An abrupt drop in resistance at the opening of the evaporator shutter and a steep rise at its closing were not due to the influence of radiation from the Ag evaporator [2].

Figure 9a shows the resistance change during cycles of Ag deposition onto the same $\sqrt{3} \times \sqrt{3}$-Ag surface at RT and its interruption [2]. Steep drops and rises in

resistance were repeatedly observed at the opening and closing of the evaporator shutter, respectively. This contrasts with the case of Au deposition in that the resistance remained constant during the interruption periods (Fig. 6a). But, as shown as the curve C in Fig. 9b, when the deposition was stopped before reaching the small overshoot in the resistance curve, the resistance remained constant even after the deposition was stopped [33]. If the deposition was prolonged beyond the overshoot, the resistance steeply recovered by stopping the deposition as shown by the curve B. Thus, there is a clear distinction in the phenomena occurring on the surface before and after the overshoot in the resistance curve. These observations can be explained by considering the dynamics of deposited Ag atoms on the surface. As mentioned before, the deposited Ag atoms were highly mobile on the $\sqrt{3} \times \sqrt{3}$-Ag surface, so that they generated a two-dimensional gas phase. Beyond a critical density in the gas phase, Ag adatoms begin to nucleate into three-dimensional islands, which are observed by using RHEED and SEM [33]. If we assume that only the two-dimensional gas phase before nucleation makes the resistance low, then the observed resistance changes are explained consistently. With less than a critical coverage Θ_C (about 0.03 ML) corresponding to the overshoot in the resistance curves in Figs. 7b and 9b, the density of Ag adatoms in the two-dimensional gas phase was too dilute to nucleate into stable nuclei. Therefore, the Ag adatoms could continue to exist separately even after the deposition was stopped, thus keeping the resistance at a small level. Beyond the critical coverage Θ_C, the Ag-adatom density became dense enough to begin to nucleate, which stopped both the increase in the Ag-adatom density on the surface and the steep resistance drop. Therefore, when the deposition was stopped at this stage, the adatoms in the gas phase were absorbed into the nuclei, thus causing most of the surface to revert to the bare $\sqrt{3} \times \sqrt{3}$ surface, which in turns causes the resistance recovery observed after the deposition was stopped. In this way, the deposited Ag atoms began to nucleate only beyond the critical density which corresponds to the "critical supersaturation" [33]. Recent Monte Carlo simulations indicate that the overshoot in the resistance curve is due to a kinetical overshoot beyond the critical supersaturation in the nucleation process [34]. *In situ* resistance measurements during depositions therefore provide important insights into the adatom dynamics on the surface not directly seen using by other methods such as microscopies.

But why do the Ag atoms only in the two-dimensional gas phase make the resistance low? One possible mechanism is a doping effect for the surafce-state band. As mentioned in Section 3, the initial $\sqrt{3} \times \sqrt{3}$-Ag surface has a characteristic surface-state band, named S_1-state band. This band plays an important role in the surafce conduction: the electrons thermally excited into this surface-state band can contribute to the electrical conduction parallel to the surface, because the S_1-state band is highly dispersive [15]. The surface charging, which is the origin of the upward band bending below this surface, is naturally understood by considering the excess electrons trapped in this S_1-state band [15]. So if the Ag adatoms in the two-dimensional gas phase on top of the $\sqrt{3} \times \sqrt{3}$-Ag surface donate the excess electrons into the S_1-state band, then the conduction through this surface-state band will be enhanced.

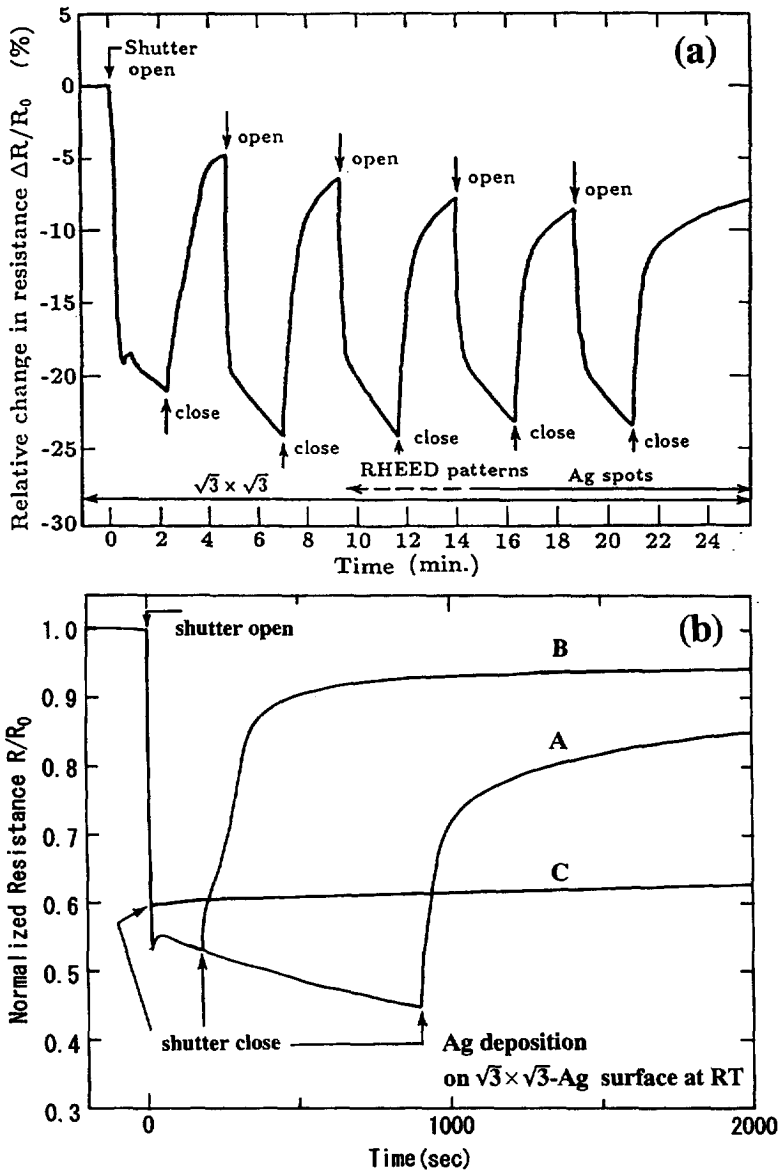

Fig. 9. Resistance change for an Si wafer with (a) $\sqrt{3} \times \sqrt{3}$-Ag surface during a cycle of deposition and interruption of additional Ag at RT. (b) Resistance changes with different amounts of additional Ag depositions.

There is other experimental data, which are suggestive of another possibility of the solution for the high conductivity. Figure 10 shows the resistance changes measured during Ag deposition onto the same $\sqrt{3} \times \sqrt{3}$-Ag surface at tempera-

tures lower than RT [35]. We used a p-type Si wafer that had $8 \sim 20\ \Omega \cdot \mathrm{cm}$ resistivity. At RT, the resistance changed in a similar way as in Fig. 7b; steep drop with less than 0.1 ML coverage, a small overshoot, and then gradual decrease with further deposition, but without any structural changes. Below 250 K, however, a $\sqrt{21} \times \sqrt{21}$ RHEED pattern appeared around 0.14 ML coverage of additional Ag [36]. In response to the emergence of this new superstructure, the resistance of the Si wafer suddenly dropped further. When the substrate was cooled, the surface migration of the deposited Ag adatoms was suppressed and fixed on particular sites on the surface. In other words, the two-dimensional gas phase was "frozen", resulting in a periodical arrangement of the adatoms making up the $\sqrt{21} \times \sqrt{21}$ superstructure. When the substrate was heated above 250 K, this $\sqrt{21}$-structure was destroyed, so that it reverted to the initial $\sqrt{3} \times \sqrt{3}$ structure; the fixed adatoms were thermally activated to nucleate into three-dimensional nuclei, thus most of the surface reverted to the initial $\sqrt{3} \times \sqrt{3}$ phase. This $\sqrt{21} \times \sqrt{21}$ structure is similar to the superstructure of the same periodicity induced by Au deposition onto the $\sqrt{3} \times \sqrt{3}$ – Ag surface at RT mentioned in Fig. 7a. Both of them were highly conductive, and temperature-variable STM observations revealed a close resemblance in images between the two [37]. Therefore, the mechanism responsible for the extremely high surface conductivity of the $\sqrt{21} \times \sqrt{21}$-Ag phase induced only at low temperatures is most likely the same as that for the surface induced by Au at RT, i.e., conduction through a metallic surface-state band. This should, of course, be confirmed by low-temperature photoemission measurements, which we are now doing. Then, what about the dramatic resistance drop observed for the Ag deposition onto the $\sqrt{3} \times \sqrt{3}$-Ag surface at RT? Our hypothesis is that although no fractional-order spots showing a $\sqrt{21} \times \sqrt{21}$ periodicity were observed in the RHEED patterns, the Ag adatoms in the two-dimensional gas phase were not randomly distributed; the $\sqrt{21} \times \sqrt{21}$-like arrangement in a short-range order formed as a transient structure, which made the resistance extremely low. The construction and destruction of this structure was continuously repeated in the gas phase, so that some fraction of the surface was always covered by the $\sqrt{21} \times \sqrt{21}$-like arrangement. To confirm this hypothesis and to find a metallic nature in the surface electronic states at RT, we are now doing the photoemission measurements for a surface on which a two-dimensional gas phase exists.

In summary, the $\sqrt{21} \times \sqrt{21}$ phase plays a key role in the conductivity changes at the initial stage of both Au and Ag depositions onto the $\sqrt{3} \times \sqrt{3}$-Ag surface. The extremely high surface conductance of this phase induced by Au adsorption is clarified to be due to metallic surface-state conduction.

5. Concluding remarks

Our results thus confirm that the electrical conductivity of a silicon crystal is crucially dependent on the surface superstructures formed on it. The 7×7 surface

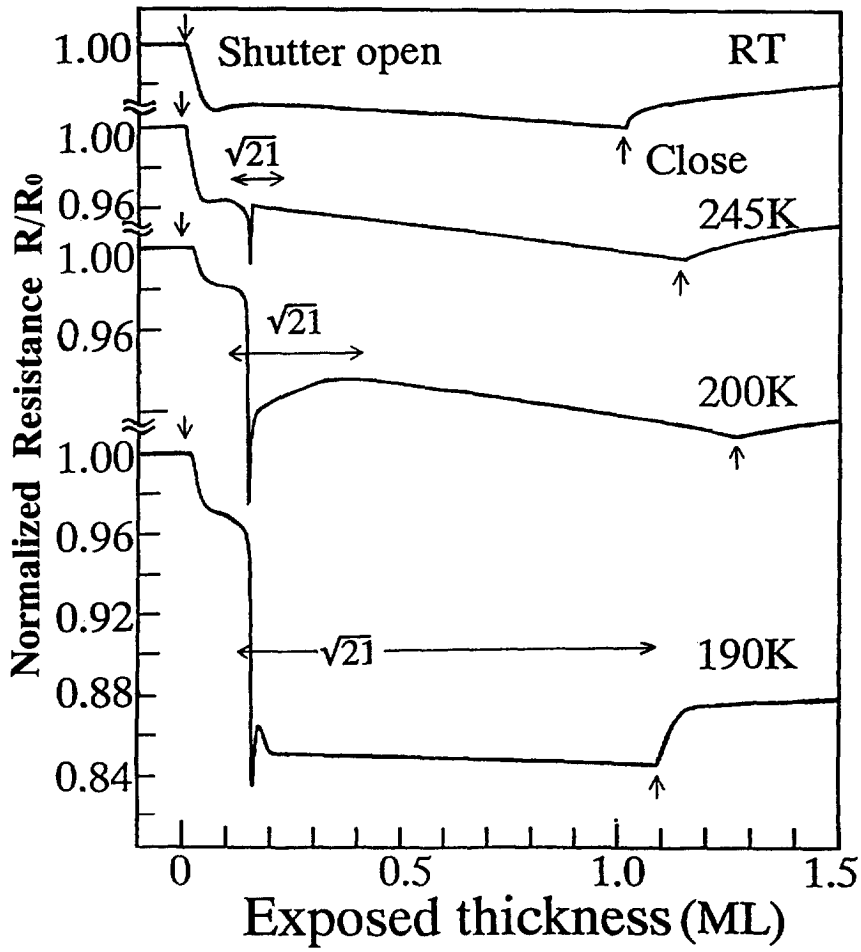

Fig. 10. Resistance changes and corresponding RHEED patterns for an Si(111) wafer with a $\sqrt{3} \times \sqrt{3}$-Ag surface during deposition of additional Ag onto the surface kept at temperatures lower than RT. The $\sqrt{3} \times \sqrt{3}$ spots were always observed in the RHEED pattern throughout all processes.

is stiff against metal adsorptions, showing no significant changes in struture and electrical conductance, while the 5×2-Au and $\sqrt{3} \times \sqrt{3}$-Ag surfaces are sensitively affected by additional metal adsorptions of much less than 1ML coverage. This is because the stacking-fault-dimer framework in the 7×7 reconstruction is much more persistent. Similar, but different in detail, phenomena are found in other metals (In, Pb) on a silicon surface; these results will be published elsewhere [38]. The resistance-change measurements for Ag adsorption on top of the Si(111)-$\sqrt{3} \times \sqrt{3}$-Ag surface, especially, demonstrate that such measurements can be used for true *in-situ* and real-time monitoring of dynamical restructuring during growths on a surface. Interpretations of the conductivity measurements, that is, the distinc-

tion among the contributions from the surface space-charge layer, the surface-state band, and the grown film, of course, need other complementary experiments such as photoemission spectroscopies.

Our results on the surface-field effect and photoconductivity, which were not discussed in this paper due to the space limitation, also indicate the decisive role of the surface superstructures in the electrical properties. We have thus found for the first time that the reconstructions only in one or two atomic layers on silicon surfaces actually raise the inherent changes in the macroscopic electrical conduction. This result will, then, lead to new ideas for devise applications. For example, imagine a domain boundary where the clean 7×7 structure and the $\sqrt{3} \times \sqrt{3}$-Ag structure adjoin on a single crystal surface, where one is metallic and the other is semiconductor-like. This is then analogous to a Schottky contact in a sense. Furthermore, the Fermi-level positions at the respective surface areas are quite different, which can be regarded as a surface version of a *pn* or *pi* junction. Therefore, this domain boundary may have certain electrical functions. Our preliminary experiments actually showed a rectifying action of this domain boundary. Then, are the electrical properties dependent on the structure of the domain boundary? This will be a new type of 'interface', and the correlation between the structures and properties have yet to be studied.

Acknowledgements

The results presented here have been obtained in collaboration with Drs. Tadaaki Nagao, Tomohide Takami, and Naoharu Shimomura, Mr. Fumio Shimokoshi, Gen Uchida, and Ms. Sakura Takeda. We also thank Profs. Shozo Ino of University of Tokyo and Martin Henzler of Hannover University for their valuable discussions. This work is supported in part by a grant-in-aid from the Ministry of Education, Science and Culture of Japan.

References

[1] J.A. Stroscio and D.M. Eigler, Science 254 (1991) 1319; M.F. Crommie, C.P. Lutz, D.M. Eigler and E.J. Hellier, Surf. Rev. Lett., 2 (1995) 127.

[2] S. Hasegawa and S. Ino, Phys. Rev. Lett., 68 (1992) 1192; Surf. Sci., 283 (1993) 438; Thin Solid Films 228 (1993) 113; Int. J. Mod. Phys., B7 (1993) 3817; in: H. Sakaki and H. Noge, (eds.), Nanostructures and Quantum Effects, Springer, Berlin, 1994, p. 104.

[3] M. Henzler, in: J.M. Blakely, (ed.), Surface Physics of Materials I, Academic Press, New York, 1975, p. 241.

[4] R. Schad, S. Heun, T. Heidenblut and M. Henzler, Phys. Rev., B45 (1992) 11430.

[5] For example, J.T. Coutts, Electrical Conduction in Thin Metal Films, Elsevier, Amsterdam, 1974.

[6] M. Jalochowski and E. Bauer, Phys. Rev., B37 (1988) 8622; Phys. Rev., B38 (1988) 5272; Surf. Sci., 213 (1989) 556.

[7] V.G. Lifshits, A.A. Saranin and A.V. Zotov, Surface Phases on Silicon, John Wiley and Sons, Chichester, 1994.

[8] K. Takayanagi, Y. Tanishiro, M. Takahashi and S. Takahashi, J. Vac. Sci. Technol., A3 (1985) 1502; Surf. Sci., 164 (1985) 367.

[9] R.J. Hamers, R.M. Tromp and J.E. Demuth, Phys. Rev. Lett., 56 (1986) 1972.
[10] F.J. Himpsel, G. Hollinger and R.A. Pollack, Phys. Rev., B28(1983) 7014.
[11] T. Takahashi and S. Nakatani, Surf. Sci., 282 (1993) 17, and references therein.
[12] Y.G. Ding, C.T. Chan and K.M. Ho, Phys. Rev. Lett., 67 (1991) 1454.
[13] T. Yokotsuka, S. Kono, S. Suzuki and T. Sagawa, Surf. Sci., 127 (1983) 35.
[14] S. Watanabe, M. Aono and M. Tsukada, Phys. Rev., B44 (1991) 8330.
[15] L.S.O. Johansson, E. Landemark, C.J. Karlsson and R.I.G.Uhrberg, Phys. Rev. Lett., 63 (1989) 2092; ibid. 69 (1992) 2451.
[16] Y.G. Ding, C.T. Chan and K.M. Ho, Phys. Rev. Lett., 69(1992) 2452.
[17] S. Kono, K. Higashiyama, T. Kinoshita, T. Miyahara, H. Kato, H. Ohsawa, Y. Enta, F. Maeda and Y. Yaegashi, Phys. Rev. Lett., 58 (1987) 1555.
[18] L.D. Marks and R. Plass, Phys. Rev. Lett., 75 (1995) 2172.
[19] I.R. Collins, J.T. Moran, P.T. Andrews, R. Cosso, J.D. O'Mahony, J.F. McGilp and G. Margaritondo, Surf. Scie., 325 (1995) 45.
[20] T. Okuda, H. Daimon, H. Shigeoka, S. Suga, T. Kinoshita and A. Kakizaki, J. Electron Spectr. Relat. Phenom., in press.
[21] L. He and H. Yasunaga, Japan. J. Appl. Phys., 24 (1985) 928
[22] M. Liehr, M. Renier, R.A. Wachnik and G.S. Scilla, J. Appl. Phys., 61 (1987) 4619.
[23] C.-S. Jiang, S. Hasegawa and S. Ino, Phys. Rev., B54 (1996) 10389.
[24] C.E. Young, J. Appl. Phys., 32 (1961) 329.
[25] A.A. Baski, J. Nogami and C.F. Quate, Phys. Rev., B41 (1990) 10247.
[26] Y. Hasegawa, I.-W. Lyo and Ph. Avouris, Appl. Surf. Sci., 76/77(1994) 347.
[27] A. Endo and S. Ino, Japan. J. Appl. Phys., 32 (1993) 4718.
[28] J.-J. Yeh, J. Hwang, K. Bertness, D.J. Friedman, R. Cao and I. Lindau, Phys. Rev. Lett., 70 (1993) 3768.
[29] A. Samsavar, T. Miller and T.-C. Chiang, Phys. Rev., B42 (1990) 9245.
[30] T. Yamanaka, A. Endo and S. Ino, Surf. Sci., 294 (1993) 53.
[31] J. Nogami, K.J. Wan and X.F. Lin, Surf. Sci., 306 (1994) 81.
[32] A. Ichimiya, H. Nomura, Y. Horio, T. Sato, T. Sueyoshi and M. Twatsuki, Surf. Rev. Lett., 1 (1994) 1.
[33] Y. Nakajima, G. Uchida, T. Nagao and S. Hasegawa, Phys. Rev., B54 (1996) No. 17, in press.
[34] A. Natori, M. Murayama and H. Yasunaga, Surf. Sci., in press.
[35] X. Tong, S. Hasegawa and S. Ino, Phys. Rev., B54 (1996) No. 19, in press.
[36] Z.H. Zhang, S. Hasegawa and S. Ino, Phys. Rev., B52 (1995) 10760.
[37] X. Tong, T. Nagao and S. Hasegawa, to be submitted to Surf. Sci.
[38] S. Takeda, X. Tong, T. Nagao, S. Hasegawa and S. Ino, to be published.